Results in Engineering 17 (2023) 100909

Contents lists available at ScienceDirect

Results in Engineering

journal homepage: www.sciencedirect.com/journal/results-in-engineering

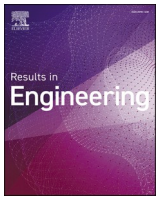

Comparative study on bubbling and shearing techniques for the crystallization of xylitol in TES systems

Miguel Navarro [a,*], Gonzalo Diarce [b,**], Ana Lázaro [a], Ander Rojo [b], Mónica Delgado [a,b,c]

[a] Aragón Institute for Engineering Research (I3A), Thermal Engineering and Energy Systems Group, University of Zaragoza, Agustín de Betancourt Building, C/María de Luna 3, 50018, Zaragoza, Spain
[b] ENEDI Research Group, Energy Engineering Department, University of the Basque Country – UPV/EHU, Plaza Ingeniero Torres Quevedo 1, 48013, Bilbao, Spain
[c] Centro Universitario de La Defensa, Academia General Militar, Ctra Huesca S/N, 50090, Zaragoza, Spain

ARTICLE INFO

Keywords:
LHTES
Crystallization
Xylitol
Bubbling
Stirring
Prototype

ABSTRACT

Xylitol is a promising phase change material for thermal energy storage at low and medium temperatures, but its supercooling and low crystallization rate can hinder its performance in actual systems. This problem can be overcome with the application of external stimuli that promotes the nucleation and subsequent crystallization of the supercooled xylitol. Seeding combined with mechanical stirring or air-bubbling, the techniques used in this study, are proven to achieve the crystallization (and the release of the stored latent heat) of xylitol, but the effect was not instantaneous. Rheological measurements were performed firstly to study the influence of shear and temperature in the crystallization of xylitol. Then, the use of different mechanisms to promote the crystallization of the material was evaluated by two different laboratory-scale prototypes; one of them included a mechanical stirring system while the other employed a gas-bubbling mechanism. Thermal power and discharged energy of xylitol were evaluated in the bubbling system prototype and the influence of supercooling in both discharged power and energy were also studied. A methodology to calculate induction time is proposed to evaluate crystallization systematically in both systems. This new systematic evaluation proposed in this work is different from that of the literature and aims to be used to compare different crystallization systems.

1. Introduction

Due to the intermittence of renewable sources, because of the dependence of these sources on climatologic variables, energy production and demand are not synced. As such, energy storage must be integrated to correct this intermittence and to reach a more flexible and sustainable energy model. Thermal energy storage (TES) is then required in thermal applications that take advantage of renewable energy sources. Latent thermal heat energy storage (LHTES) systems show a high energy storage density; as the materials used in these systems, phase change materials (PCM) can store up to 6 times more energy than sensible heat materials, by units of volume [1] such as water vs xylitol in a temperature range of 15 °C.

Sugar alcohols are phase change materials (PCMs) with a remarkable potential for low-to-medium temperature latent thermal energy storage (LHTES) applications: they possess high phase change enthalpies in comparison to other PCMs, they are safe, sustainable, and show reasonable prices [2]. As such, there are many new studies on sugar alcohols, such as erythritol [3–6]; mannitol [7–9], or sorbitol [10–12]. Some of the applications for sugar alcohol-based thermal energy storage systems are solar concentration [9,13] and waste heat applications [14].

Amongst them, xylitol (melting point: 92 °C) presents the mentioned good thermophysical properties, but it also shows a noticeable and stable supercooling coupled with a low crystallization rate [15]. There are many works that study the properties of xylitol, such as viscosity, density, or melting temperature [2,15–19]. There are, however, discrepancies in the results between studies [17,20,21]. The stable supercooling leads to difficulties to nucleate on cooling and, when it does, it shows a low heat release rate; however, this behaviour enables the opportunity to develop heat storage applications based on stable supercooling, in which the PCM remains in the supercooled state until the heat release is required. Then, crystallization is promoted on demand by an external stimulus [22]. Some works take advantage of supercooling to control the process, such as [22–24]; but other authors study means of

* Corresponding author.
** Corresponding author.
E-mail addresses: 702550@unizar.es (M. Navarro), gonzalo.diarce@ehu.eus (G. Diarce).

https://doi.org/10.1016/j.rineng.2023.100909
Received 20 October 2022; Received in revised form 16 December 2022; Accepted 11 January 2023
Available online 21 January 2023

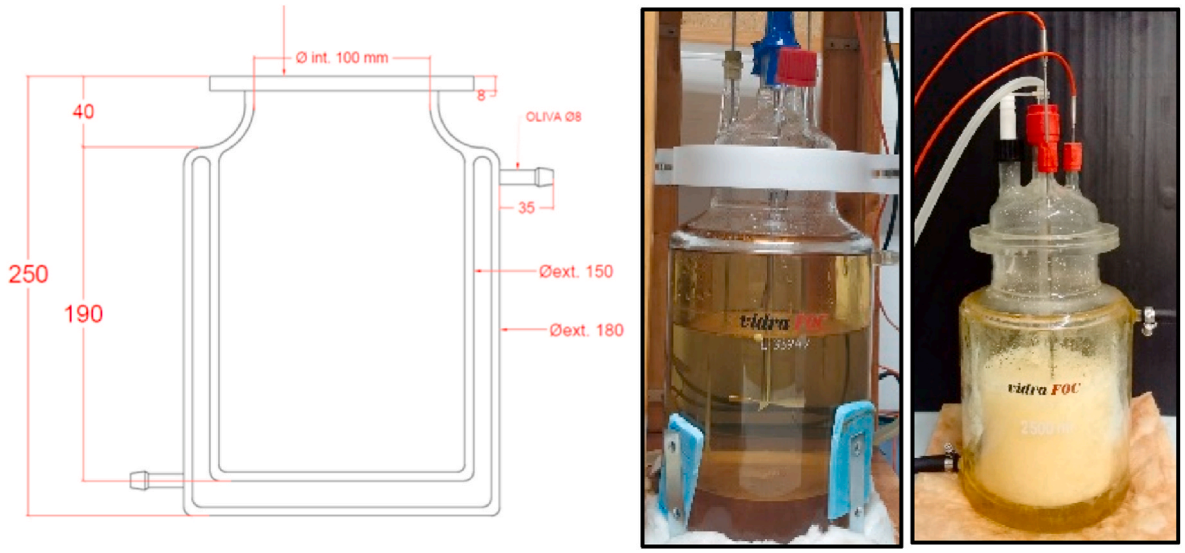

Fig. 1. Employed prototypes: main dimensions (left), mechanically stirred prototype (centre), and bubbling system prototype (right).

triggering crystallization by reducing supercooling [25–27]. Thus, to successfully operate a heat storage system using supercooled PCMs, the initiation of the crystallization process and the achievement of high crystallization rates are critical parameters to be controlled.

Crystallization consists of two different processes: nucleation (the formation of new crystals in the sample) and crystal growth. The nucleation process is also divided into two processes: primary nucleation, where crystals form from the melt, and secondary nucleation, where nuclei are formed from already existing crystals. Usually, secondary nucleation rapidly becomes the principal force of crystallization in a crystallization process after primary nucleation has formed enough nuclei [28,29]. Secondary nuclei can be formed by contact between crystals, contact with a surface, or fluid shear [30,31]. Shear promotes crystallization in a highly saturated solution until a maximum in crystallization rate is reached [32].

Several techniques have been studied to promote nucleation in sugar alcohols, such as shearing [1], adding additives [33], bubbling [34,35] or ultrasound [36]. Of these, stirring by bubbling [34] and/or mechanical shearing [1,37] might be adequate as they can also cause a fast crystallization of the material and thus induce an appropriate heat release velocity. To gain further knowledge of the advantages and disadvantages of these activation techniques, the present paper presents the preliminary results of two laboratory-scale prototypes, each including one of the mentioned activation systems. In addition, experiments performed by a rheometer are presented to broaden the understanding of the crystallization of xylitol by shearing.

The results of a similar experimental setup were recently published in Picard et al. [37]. In that work, bubbling and mechanical stirring were applied to study the crystallization of xylitol in a prototype comparable to the ones herein presented; however, the applied bubbling flow rate and the rotation speed were not the same. The prototype volume used was also different (4.5 times lower) and the gas used for bubbling was N_2, while we used air. Considering the differences in the experimental conditions, plus the fact that crystallization from a supercooled melt is a stochastic effect; the results presented here are valuable to complement those presented in Ref. [37].

2. Materials and methods

2.1. Materials

Xylitol (99% purity) was used in both institutions. Its formula is $C_5H_{12}O_5$ and its CAS number is 87-99-00. The main physical properties of xylitol are: density of 1.52 g/ml (in liquid state), melting point 94.3 °C, and latent heat of 239.3 J/g [2]. Xylitol, as do other sugar alcohols, shows a supercooled state; thus, the liquid phase can be observed at temperatures below the melting temperature and, at the same time, xylitol also has a low crystallization rate [15]. Xylitol seeds used to promote the crystallization had a radius of between 315 and 400 μm. These seeds were obtained by sieving xylitol chunks as directly received.

2.2. Rheological measurements

To study the crystallization of xylitol, an AR-G2, stress-controlled rheometer from TA Instruments was used. The rheological system used with the rheometer was a Peltier plate with a 40 mm diameter parallel plate geometry, as the Peltier plate can be used to control the temperature of the sample. This system has two main drawbacks. The first is the temperature gradient between the Peltier plate and the parallel plate, as the geometry is not a heated geometry, which causes the small gradient in the sample, and which can affect the viscosity measured by the rheometer. This difference in temperature causes differences in viscosity values. In this sense all the effects of this temperature problem which cause the deviation in viscosity, is studied by doing measurements with a standard oil. Experiments performed with standard oil deviated by 8% from the certified value (at 80 °C). At higher temperatures, deviation is greater than at low temperatures.

The second is that the shear rate is dependent on the radius of the parallel plate geometry and the maximum shear rate is located at the edge of the geometry.

For the experiments presented in this paper, three different shear rates and temperatures were chosen. The shear rates were 5, 10, and 15 s^{-1} at the edge of the geometry, and the temperatures were 70, 80, and 90 °C. The selected shear rates were lower than 20 s^{-1} since it was observed that, at 20 s^{-1}, crystal disaggregation occurred because of high shearing, which can hinder crystallization [1]. The maximum crystallization rate for xylitol was observed at 70 °C [15]. The gap (xylitol sample's height, distance between the Peltier plate and the parallel plate geometry) selected for the experiments was 600 μm, larger than the seed size used to activate crystallization, but small enough to lessen the temperature gradient of the sample. Xylitol seeds had a diameter between 315 and 400 μm, obtained by sieving xylitol chunks.

To ensure that the parallel plate geometry was not in contact with the seed, the sample was loaded in different steps. First, half of the xylitol was added and melted on the Peltier plate. Then, the temperature was lowered to the experiment temperature and a seed was added. Next, the

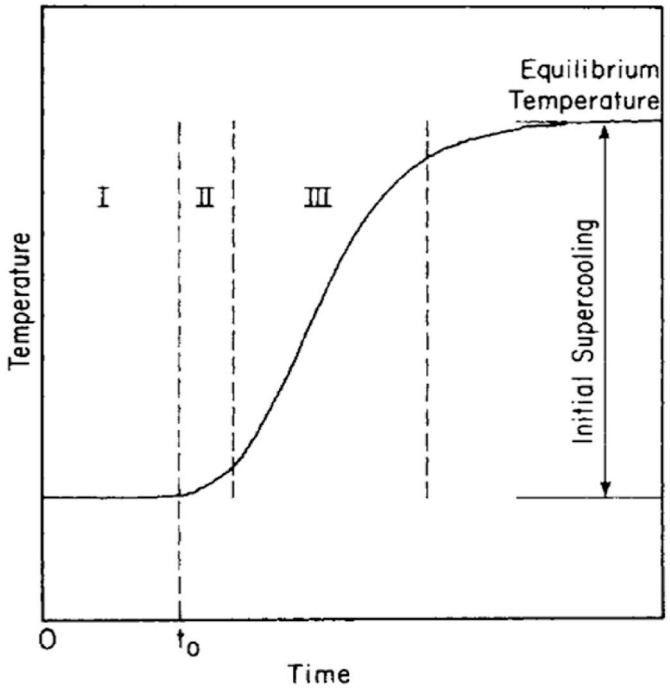

Fig. 2. Change in temperature of an exothermic crystallization process [38].

remaining half of the xylitol, previously melted in an oven, was loaded. Finally, once the geometry was in position, the experiment started.

2.3. Main characteristics of the prototypes used (mechanical stirring and bubbling systems)

Two equivalent prototypes were used for the experiments, each with a different activation system. Their main body consisted of a cylindrical glass vessel that held the xylitol inside, with a diameter of 150 mm and a height of 250 mm (Fig. 1). The total inner volume was 3.35 L and 2.5 kg of xylitol were used. To control the temperature of the xylitol and the system charge/discharge, the inner vessel was surrounded by a glass heating jacket (180 mm diameter) that allowed the flow of a heat transfer fluid (HTF), silicone thermal oil. This heating jacket was connected by hoses to a thermostatic bath, which controlled the temperature and mass flow rate of the HTF.

The two activation systems used were based on bubbling and stirring mechanisms, respectively. The bubbling activation system consisted of a glass cannula with an inner diameter of 1.2 mm that was immersed in the PCM to introduce air from the bottom of the vessel. A rotameter controlled the air flow rate. The stirring activation system was formed by an impeller (IKA Eurostar 60 digital) placed in the centre of the tank. Its stirring rate was 100 rpm. In both prototypes, the temperature of the xylitol was registered by two Pt-100 immersed in the bulk PCM at different heights. The inlet and outlet temperatures of the HTF were recorded by temperature probes. The lid of the tank has a special hole to drop the seeds on the upper surface of the supercooled xylitol.

2.4. Operation conditions of the experiments performed with the prototypes

The performed tests consisted of an initial melting of the xylitol by heating the material up to 205 °C, followed by a cooling process down to a specific temperature below the melting point of the material (i.e.: a supercooled state). After isothermal conditions were achieved, the activation mechanism was turned on and, in selected cases, xylitol seeds were added to help promote the nucleation. The inlet temperature of the HTF was kept constant at the specified value during the whole process. Tests with various supercooling degrees were performed: in the mechanically stirred prototype, the starting temperatures ranged from 60 °C to 80 °C (at every 5 °C), while in the bubbling system, they ranged from 45 to 80 °C. The lowest chosen temperature in the stirred prototype was 60 °C because, at lower temperatures, the increasing viscosity of xylitol caused the Pt-100 probes to swirl with the liquid in movement, which was dangerous for the temperature sensors.

2.5. Induction time definition

Induction time is used to compare experiments at different temperatures. Induction time is defined as the time between the introduction of the stimulous and the increase in temperature of the crystallization system. In an exothermic reaction event, there are three different stages [38,39] which can be seen in Fig. 2. In the first stage, the temperature remains constant, even though nuclei are already being formed. The second stage is formed by the early rise of the temperature, and the third stage lasts from the end of the second stage until the temperature reaches equilibrium.

To measure the induction time, a small increment of temperature in the system can be used [38,39]. The induction time is then calculated as the time from the crystallization stimulus until the temperature has augmented in a fixed increment. (In the case of Omran et al. (1974) [38] the increase taken is 0.005 °C and in Picquard et al. (2022) [37] the increment is defined as 0.05 °C. In this work, the calculation of the induction time is calculated by the intersection between the initial

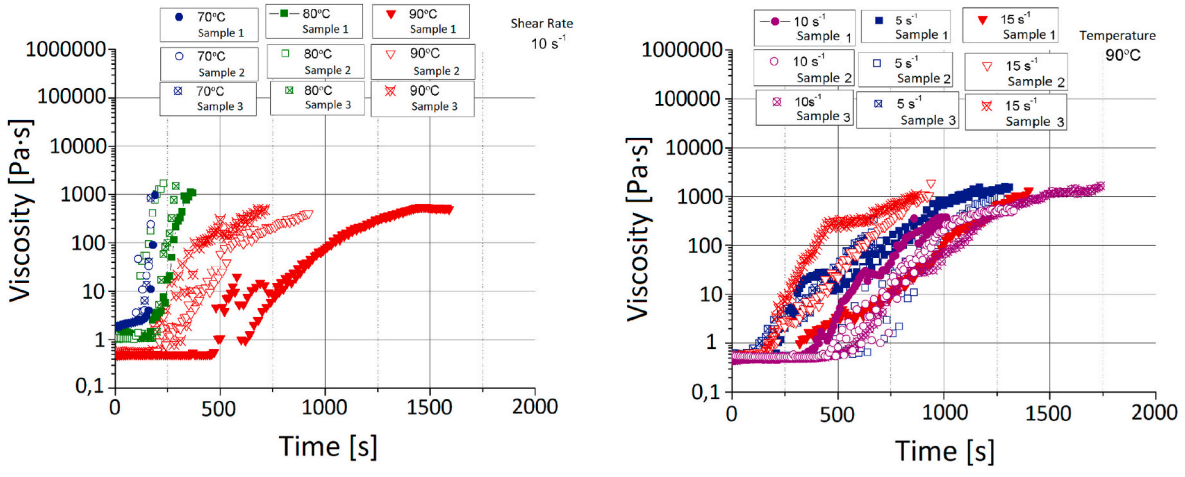

Fig. 3. Evolution of the viscosity of xylitol at different working temperatures (left) and with different shear rates (right).

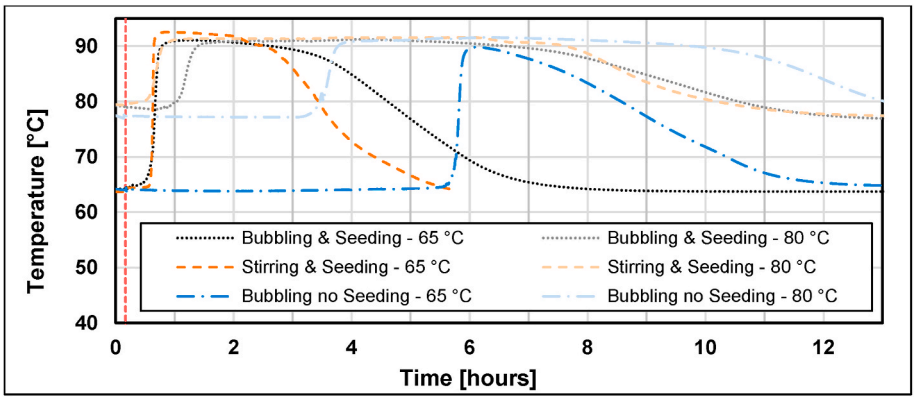

Fig. 4. Temperature evolution of xylitol for different HTF operation temperatures.

temperature, and the tangent at the inflection point of the curve. By using the inflection points of the curves, this new method allows the comparison of different systems; as it is not reliant on the precision of the temperature sensor.

Akin to the temperature curve, three different zones can be appreciated in the measurements. The first (induction zone) occurs at the beginning of the measurement, where viscosity remains constant. The second (crystallization zone) is triggered when crystallization starts. It can be recognized as a sudden increase in the viscosity and finishes when the end of the experiment is reached, or when the third zone starts. This third (slip zone) emerges when the viscosity is no longer increasing or is increasing at a much lower rhythm than at the start of the second zone. This occurs when the sample is fully crystallized but rotates along with the geometry.

3. Results and discussion

First, the rheological experiments are presented, followed by the results obtained with the prototypes regarding induction time, discharged energy, and thermal power.

3.1. Rheological results: influence of temperature and shear on xylitol crystallization

The results from the rheometer can be seen in Fig. 3, which shows the effects of the temperature (left) and shear rate (right) on the crystallization of xylitol. Note that, to achieve the crystallization, a seed was required even if the xylitol was sheared. Once crystallization had been activated, the induced shear on the xylitol promoted crystallization [36].

The influence of temperature on crystallization can be observed in Fig. 3 (left). First, the induction time was assessed; this is the time elapsed from the beginning of the stimulus (shear) until the temperature of the xylitol rises, i.e.: the time required for the crystallization to start. A clear trend is appreciated in the figure: at 70 °C, induction times were shorter than at 80 °C and 90 °C; however, the results at 90 °C showed wide scattering. This can be because crystallization has a stochastic nature.

The crystallization rate of xylitol can be assessed from the slope of the crystallization zone. As observed in the figure, the lower the temperature, the more pronounced the slope. This indicates that the crystallization rate was faster at 70 °C than at 80 and 90 °C. These results are consistent with the literature [15].

The results of the different shear rates are presented in Fig. 3 (right). Again, the scattering in the induction time was noticeable, as observed above. However, based on the similar slopes of the different measurements, the tested shear rates (5, 10, and 15 s^{-1}) had no significant influence on the crystallization rate of the xylitol.

3.2. TES prototype results: induction time

The temperature evolution of the xylitol was analysed in the experiments to estimate the induction time (see definition in Section 3.1). It is important to remark that, with no stimulus, xylitol can remain supercooled for days; although, as explained below, spontaneous crystallization sometimes occurred. This was probably caused by the presence of impurities within the PCM.

In Fig. 4, the temperature evolution of selected experiments at different HTF operation temperatures is presented. The red dashed vertical line at the beginning of the process represents the starting time of the stimulus. As observed, in every curve, the temperature of the xylitol started stable in a supercooled state until a sudden increase

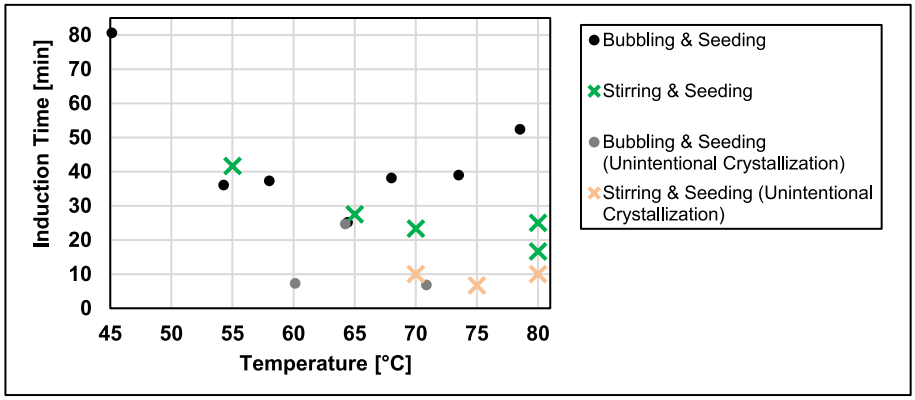

Fig. 5. Induction time vs. temperature for experiments with seeding.

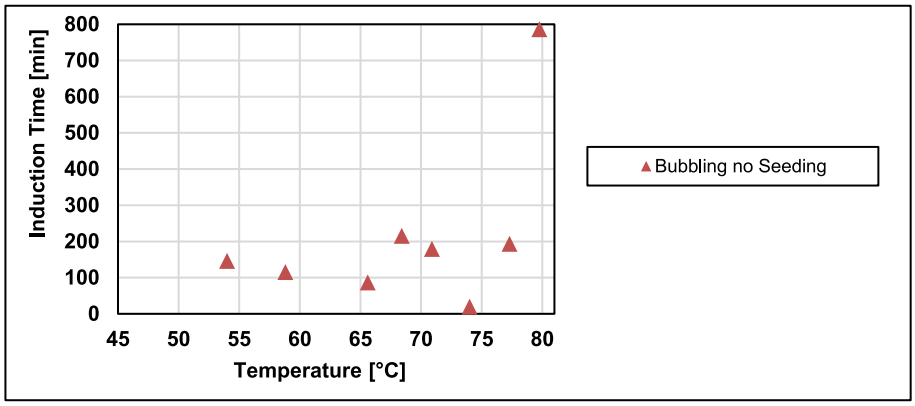

Fig. 6. Induction time vs. temperature for experiments with no seeding.

occurred until the temperature reached around 92 °C, which is the melting temperature of the PCM. This phenomenon is known as recalescence. The induction time was calculated for every experiment by crossing the lines tangential to the supercooled isothermal segment and the temperature increases during recalescence, as defined in the 2.5 section.

The induction times for the different HTF operation temperatures were analysed, and grouped by experimental conditions. The results are shown in Fig. 5 (with seeding) and Fig. 6 (without seeding).

Regarding the results that included seeding (Fig. 5), the bubbling mechanism showed a clear dependence on the working temperature, forming a parabolic shape with a minimum value of around 65 °C. This is consistent with traditional crystallization theories, which state that there is an optimum temperature below the melting point where nucleation is more likely to occur. Below this temperature, nucleation is hindered by an excessive increase of viscous forces, while above this temperature the effect is not likely to happen due to an insufficient supersaturation of the melt. Furthermore, it was noticed that the minimum absolute value of the induction time was around 25 min, which might be considered excessive for real TES systems.

On the contrary, mechanical stirring did not show such a marked dependency on temperature for the induction time and the absolute values were generally lower than the bubbling system. The minimum induction time was around 20 min and occurred at 80 °C. Further experiments are required to confirm this behaviour.

In some experiments, unintentional crystallization was noticed, which showed lower induction times than those presented above. Even though this effect might seem beneficial, it would introduce considerable uncertainty at the discharge control for real storage systems. An increased number of experiments is required to acquire further knowledge on this effect, which is currently underway.

The temperature distribution within the bulk PCM was also monitored during the experiments and evaluated (not shown in the figures above). It was noted that the crystallization with the bubbling system showed a more homogeneous temperature distribution than with mechanical stirring. Even though this effect does not influence the induction time trends obtained, it could be useful to optimize the operation parameters that affect the heat transfer within the PCM for TES purposes (e.g.: the shear rate, dimensions of the impeller, amount of bubbling inlet points required, etc.).

Concerning the results with no seeding (Fig. 6), it is worth noting that crystallization was not achieved with the mechanical stirring system in any of the HTF operation temperatures. Conversely, crystallization was achieved with the bubbling mechanism, although the induction times were noticeably longer and less reproducible than with seeding. In addition, no significant dependency on temperature was observed.

3.3. Discharged energy and thermal power

The evolution of the released energy and power during the discharge of the system was solely assessed for the experiments with bubbling, due to experimental complications during the set-up of the mechanical stirring prototype. To study the thermal behaviour of the system, the thermal power released from the xylitol to the thermal oil was calculated by Eq. (1), for every recorded time step. The contribution from the air stream used for bubbling was neglected in the balance, due to the difficulty of measuring its temperature. However, the estimations performed showed that the theoretical maximum energy the air could remove from the system was insignificant for the operating conditions involved, in comparison with the other heat exchanges involved.

$$\dot{Q}_{Xyl} = \dot{m}_{oil} \cdot c_{p\ oil} \cdot (T_{oil\ out} - T_{oil\ in}) + |\dot{Q}_{loss}| \quad (1)$$

where $\dot{Q}_{oil}$ (W) is the thermal power released by the xylitol, $\dot{m}_{oil}$ (kg/s) is

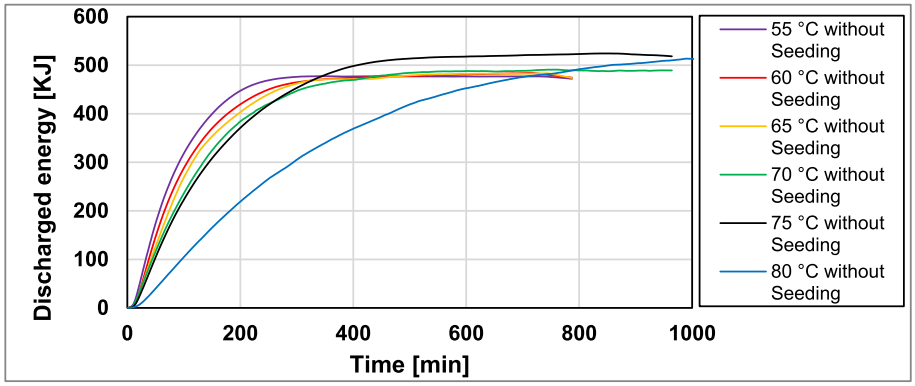

Fig. 7. Discharged energy for the bubbling system at different temperatures (no seeding).

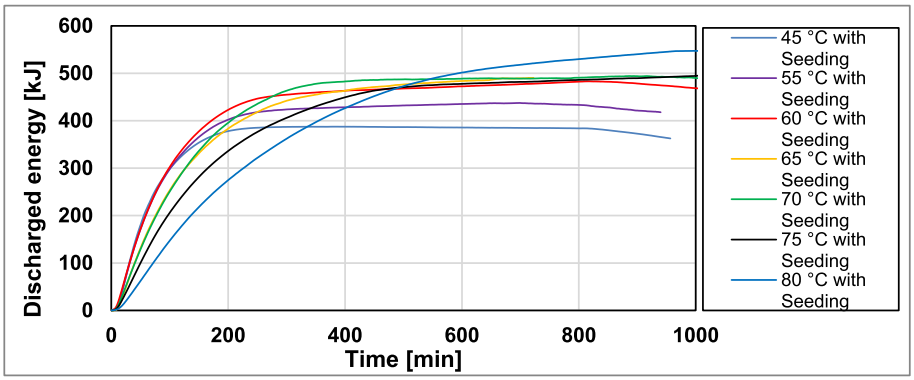

Fig. 8. Discharged energy for the bubbling system at different temperatures (with seeding).

Table 1
Energy released by xylitol, discharge time, and maximum power during the tests with bubbling.

	Discharged energy [kJ]		Discharging time for specific discharge ratios [min]		Max. Power [W]
HTF inlet temperature (°C)	Theoretical -ref. [2] (for m = 2.5 kg)	Measured	95%	90%	
Without seeding rowhead					
55	495.3	477.3	210.0	177.5	82.3
60	507.7	484.0	277.5	222.5	69.7
65	520.3	482.6	288.3	240.0	57.9
70	533.0	491.0	370.0	289.2	52.9
75	545.8	524.2	398.3	332.5	48.5
80	558.5	518.0	801.7	655.0	23.1
With seeding rowhead					
45	471.4	387.5	173.3	143.3	91.9
55	495.3	437.5	237.5	183.3	79.2
60	507.7	483.1	340.8	220.0	75.4
65	520.3	447.1	410.8	297.5	60.9
70	533.0	494.3	315.8	265.0	56.5
75	545.8	496.8	510.0	392.5	43.9
80	558.5	547.4	714.2	561.7	31.6

the mass flow of the oil used as heat transfer fluid, $c_{p\ oil}$ (J/(g·K)) is the specific heat of the oil used as heat transfer fluid, $(T_{oil\ out})$ and $(T_{oil\ in})$ (°C) are the outlet and inlet temperatures of the oil circulating in the external jacket of the tank, and $\dot{Q}_{loss}$ (W) is the thermal losses estimated for the inlet temperature of the oil. The thermal losses in equation (1) were not monitored, but estimated from a correlation obtained for every experiment. To do so, the thermal losses to the ambience in two specific isothermal segments of the experiments were calculated: first, when the system was fully charged above the melting temperature and, second, when the system was totally discharged. In both isotherms, the system was considered to be in steady state, so (Eq. (2)) could be applied. To ensure a steady state in xylitol, temperature was controlled and it was checked if xylitol temperature was constant before doing the measurement. The HTF (heat transfer fluid) is controlled to ensure xylitol remains at the experiment temperature, and does not cool until room temperature. Between these two points, the thermal losses were assumed to be linear. The resulting correlation was used to estimate the instantaneous thermal losses in equation (1).

$$\dot{Q}_{loss} = \dot{m}_{oil} \cdot c_{p\ oil} \cdot \left(T_{oil\ out} - T_{oil\ in\ steady\ state}\right) \quad (2)$$

Where $T_{oil\ in\ steady\ state}$ (°C) is the inlet temperature of the oil circulating in the jacket. The energy exchanged was obtained by integrating the instantaneous thermal power values.

3.3.1. Discharged energy

The timewise evolution of the discharged energy for the studied conditions is shown in Fig. 7 (no seeding) and Fig. 8 (with seeding), for the experiments with the bubbling prototype. The origin of abscissae (t = 0) in both figures corresponds to the beginning of the recalescence process, which means that the initial isothermal segment under the supercooling conditions shown in Fig. 4 is not represented therein.

The illustrations are complemented with Table 1, where the numerical values of the energy released by the PCM are provided. These are accompanied by the theoretical energy that the xylitol should release between the involved temperature ranges. This energy was estimated from DSC results published in previous references. Furthermore, the time needed to discharge the system for two specific discharge ratios was included, as well as the maximum power registered during the tests (the latter parameter is discussed in Section 3.3.2).

In the theoretical calculation of energy discharged by xylitol, it is assumed that part of the latent heat liberated is used to heat the supercooled xylitol to the melting point temperature. After the phase change is finished, energy is still discharged because of the temperature difference between solid xylitol and the HTF. Because the specific heat of liquid xylitol is much greater than the specific heat of solid xylitol, the supercooling effect in the theoretical energy calculation is not negligible. The formula used to calculate the theoretical energy for the experiment i $E^i_{therotical}$ is:

$$\begin{aligned} E^i_{therotical} &= m_{xyl} \cdot \left[\Delta H_{xyl} - \overline{c}_p^{liq} \cdot \Delta T^i_{sub} + \overline{c}_p^{sol} \cdot \Delta T^i_{sub}\right] \\ &= m_{xyl} \cdot \left[\Delta H_{xyl} + \left(\overline{c}_p^{sol} - \overline{c}_p^{liq}\right) \cdot \Delta T^i_{sub}\right] \end{aligned} \quad (3)$$

Where m_{xyl} is the xylitol mass of the tank, ΔH_{xyl} is the latent heat of xylitol, ΔT^i_{sub} is the supercooling of xylitol, equal to the difference between melting point and the initial temperature of the experiment i, and $\overline{c}_p^{sol}$, $\overline{c}_p^{liq}$ are the average specific heat of solid and liquid xylitol, respectively, between the supercooled temperature and the melting temperature. It is worth to highlight that the difference between the liquid and solid specific heat makes the total energy discharged less than the theorical latent heat.

As observed, the theoretical and measured discharged energies are reasonably in agreement. In addition, the total amount of energy released by the system depends on its working temperature: the lower the HTF operation temperature, the lower the amount of energy discharged. This is an expected result since, for increased levels of supercooling, a higher amount of energy stored within the PCM must be invested in the recalescence of the material. However, the trend was more pronounced for the results with seeding, while the tests without seeding show a lower dependency on temperature. This effect was not attributed to physical reasons but to experimental uncertainties. Since the experiments with seeding were shorter (due to the shorter induction times), the accumulated error in the heat loss estimation over time was

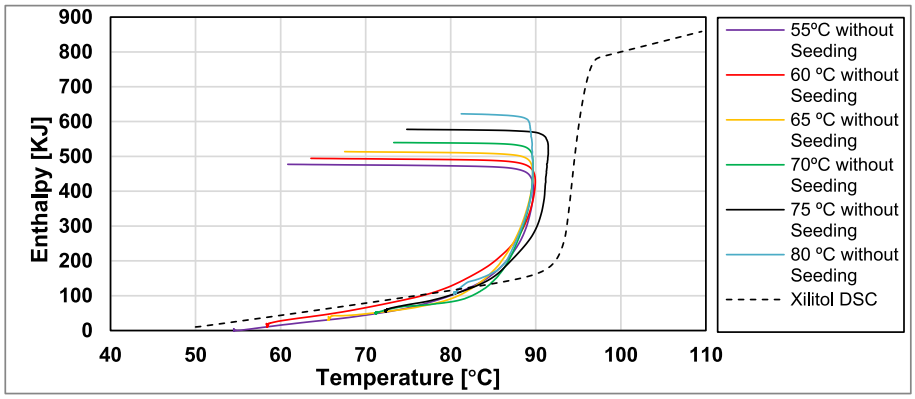

Fig. 9. Enthalpy – temperature curve of the xylitol obtained from experiments (without seeding).

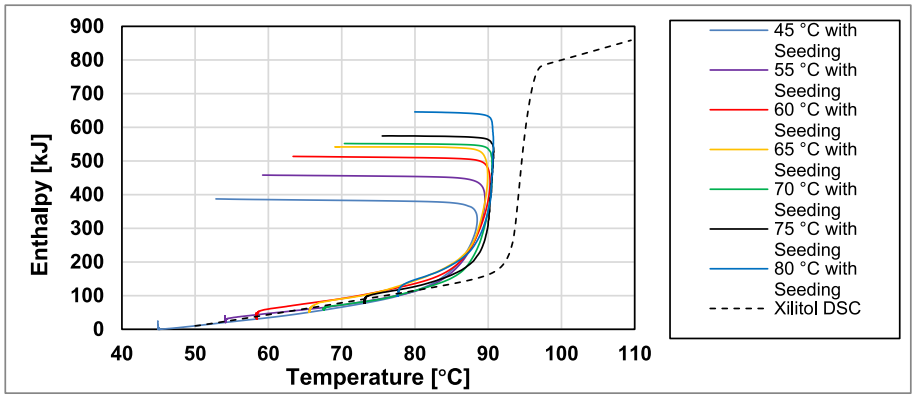

Fig. 10. Enthalpy – temperature curve of the xylitol obtained from experiments (with seeding).

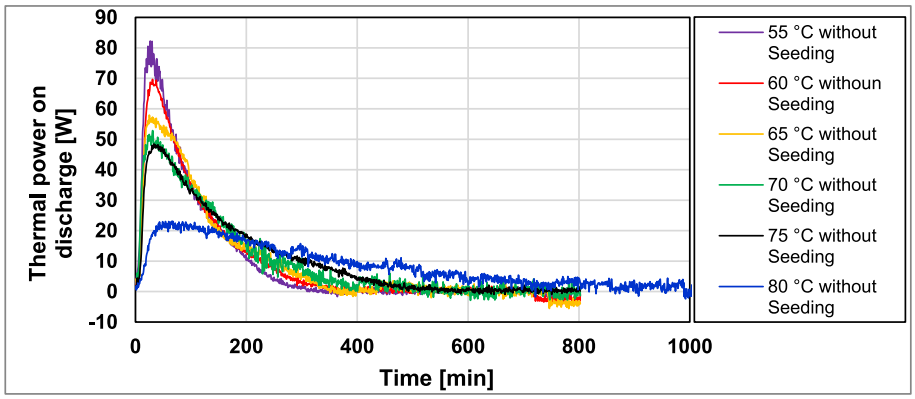

Fig. 11. Thermal power during discharge of the system at different temperatures (no seeding).

also lower. This would render more accurate results when performing the energy balances of the system.

In terms of the time required to complete the discharge from the beginning of the recalescence, the system was able to complete its discharge faster at lower temperatures. In other words, the thermal power was higher at lower operating temperatures (this aspect is discussed in more detail in the next subsection).

The xylitol enthalpy-temperature curves obtained during the experiments are presented in Fig. 9 (without seeding) and Fig. 10 (with seeding). The curves were built by setting the enthalpy reference point (H = 0 kJ) at 45 °C for every experiment. In addition, for comparison purposes, the enthalpy temperature curve for the melting of xylitol by DSC is presented with a black dashed line (note that the curve for solidification cannot be attained by DSC, since crystallization does not occur unless a stimulus is employed). These curves are helpful to see, at a glance, how much energy can be stored/released between two specific HTF operation temperatures. The curves have the same form as the discharged process represented on the enthalpy-temperature map by del Barrio et al. (2017) [20].

3.3.2. *Thermal power*

The thermal power during the induction and recalescence time was analysed by Eq. (1). The timewise results are shown in Fig. 11 (without seeding) and Fig. 12 (with seeding). (Note that the TES prototype employed is not optimized for thermal power behaviour, so the absolute values obtained are not representative of the achievable power in a real

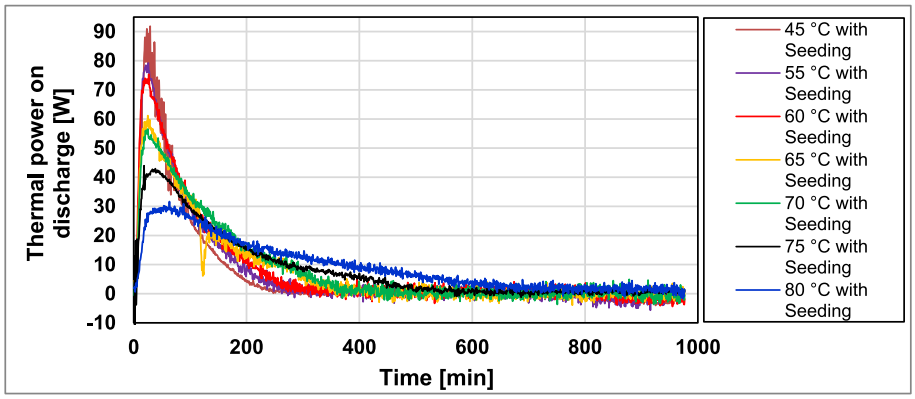

Fig. 12. Thermal during discharge of the system at different temperatures (with seeding).

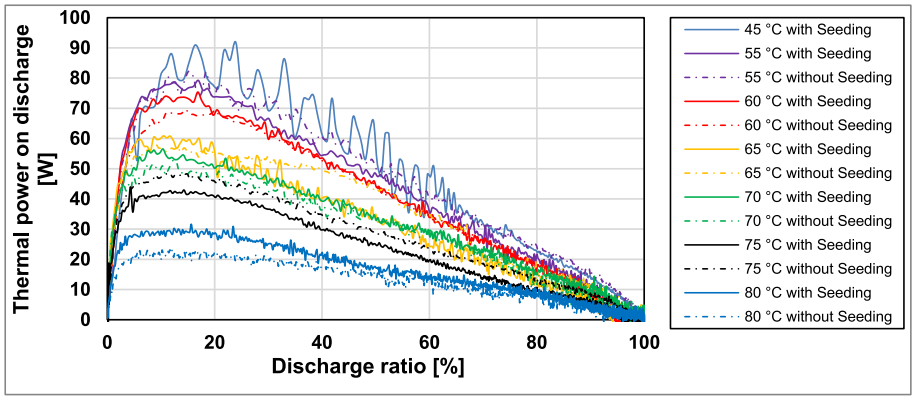

Fig. 13. Thermal power on discharge vs. TES discharge ratio, for different HTF operation temperatures.

TES system)

For every HTF operation temperature, the discharging power follows a similar profile, with a noticeable and sharp peak at the beginning (caused by the recalescence of the xylitol), followed by a gradual power decrease. For the different temperatures, the peak of maximum power is higher for lower HTF operation temperatures. This is expected since, in theory, for a system with the same PCM, the thermal power must be proportional to the temperature difference between the material and the heat transfer fluid.

However, the differences in the maximum power achieved are not evenly distributed for the different HTF operating temperatures tested. In Fig. 11 and 12, it can be observed that there is no significant difference between the power peak value at 65, 70, and 75 °C; however, between these three temperatures and 80 °C, there is a noticeable difference in the power peak values. A similar effect occurs if we compare the power peak values at the mentioned temperatures with those at 55 and 60 °C. These trends suggest that the crystallization rate, whose maximum is around 70 °C [15], also influenced the thermal power achieved.

Another observation raised from Fig. 11 and 12 is that the thermal power for the different temperatures crosses at a certain point; however, this does not mean that, at some point, the thermal power at lower HTF operation temperatures is larger than at higher temperatures. This occurs because the results are represented timewise. Thus, the charging ratio value at every time is not the same for the different curves presented. Thus, in Fig. 13, the thermal power on discharge is plotted against the PCM discharge ratio for every test. As can be seen there, the thermal power at lower HTF operation temperatures is maintained higher at every discharging ratio during the whole experiment. This is consistent with the theoretical behaviour of thermal power, which has to be larger for higher temperature differences between the PCM and the HTF.

4. Conclusions

- Either bubbling or mechanical stirring promotes and accelerates the crystallization rate in xylitol-based TES systems. However, regardless of the stimulus, crystallization is not instantaneous; the achieved minimum induction time (without unintentional seeding) was around 20 min.
- The induction times with the bubbling mechanism showed a clear dependence on the working temperature, conversely to the system with mechanical stirring. Induction time results were more reproducible when seeding was used.
- With bubbling, crystallization was achieved with no seeding, although induction times are noticeably longer than with seeding. By mechanical stirring, crystallization did not occur unless seeding was employed.
- Unintentional crystallization occurred in some experiments, which showed lower induction times. Further research is required to understand this effect.
- The measured discharged energies along the experiments were in good agreement with the theoretical capacity values of xylitol obtained from DSC.
- The thermal power on discharge mainly depends on the temperature difference between the HTF and the PCM, as expected; however, the crystallization rate might also influence it.

Credit author statement

Miguel Navarro. Conceptualization, Methodology, Investigation, writing, data cleaning, Formal analysis, Visualization. Gonzalo Diarce.

Conceptualization, Methodology, writing and review, Supervision. Ana Lázaro. Conceptualization, Methodology, writing and review, Supervision, Project administration, Funding acquisition. Ander Rojo. Conceptualization, Methodology, Investigation, writing, data cleaning, Investigation, Formal analysis, Visualization. Mónica Delgado. Conceptualization, Methodology, experimentation, review.

Declaration of competing interest

The authors declare the following financial interests/personal relationships which may be considered as potential competing interests: Miguel Navarro, Gonzalo Diarce, Ana Lazaro, Ander Rojo, Monica Delgado reports financial support was provided by State Agency of Research.

Data availability

Data will be made available on request.

Acknowledgments

This work has been partially financed by the State Research Agency (SRA) and European Regional Development Fund (ERDF). Research Projects: PID 2020-15500RB-I00, TED2021-131061B–C31, and TED2021-131061B–C32.Miguel Navarro acknowledges the funding from the Ministry of Science, Innovation and Universities of Spain through the grants for pre-doctoral contracts for the training of doctors contemplated in the State Training Subprogramme of the State Programme to Develop, Attract and Retain Talent, within the framework of the State Plan for Scientific, Technical and Innovation Research 2021–2023, reference PRE2021-097131.The authors would like to acknowledge the use of the Servicio General de Apoyo a la Investigación-SAI, Universidad de Zaragoza.

References

[1] M. Delgado, M. Navarro, A. Lazaro, S. Boyer, E. Peuvrel, E. Peuvrel, Triggering and acceleration of xylitol crystallization by seeding and shearing: rheo-optical and rheological investigation, Sol. Energy Mater. Sol. Cells 220 (2021), 110840, https://doi.org/10.1016/j.solmat.2020.110840.

[2] E. Del Barrio, R. Cadoret, J. Daranlot, F. Achchaq, New sugar alcohols mixtures for long-term thermal energy storage applications at temperatures between 70 °C and 100 °C, Sol. Energy Mater. Sol. Cells 155 (oct. 2016) 454–468, https://doi.org/10.1016/j.solmat.2016.06.048.

[3] K. Turunen, M. Yazdani, A. Santasalo, A. Seppala, Exceptional cold-crystallization kinetics of erythritol-polyelectrolyte enables long-term thermal energy storage, Sol. Energy Mater. Sol. Cells 230 (sep. 2021), 111273, https://doi.org/10.1016/j.solmat.2021.111273.

[4] K. Turunen, M. Yazdani, S. Puupponen, A. Santasalo, A. Seppala, Cold-crystallizing erythritol-polyelectrolyte: scaling up reliable long-term heat storage material, Appl. Energy 266 (may 2020), 114890, https://doi.org/10.1016/j.apenergy.2020.114890.

[5] S. Puupponen, A. Seppala, Cold-crystallization of polyelectrolyte absorbed polyol for long-term thermal energy storage, Sol. Energy Mater. Sol. Cells 180 (jun. 2018) 59–66, https://doi.org/10.1016/j.solmat.2018.02.013.

[6] S. Puupponen, V. Mikkola, T. Nissila, A. Seppalaa, Novel microstructured polyol–polystyrene composites for seasonal heat storage, Appl. Energy 172 (jun. 2016) 96–106, https://doi.org/10.1016/j.apenergy.2016.03.023.

[7] A. Paul, A. Paul, A. Paul, L. Shi, C. Bielawski, A eutectic mixture of galactitol and mannitol as a phase change material for latent heat storage, Energy Convers. Manag. 103 (oct. 2015) 139–146, https://doi.org/10.1016/j.enconman.2015.06.013.

[8] A. Sagara, T. Nomura, M. Tsubota, N. Okinaka, T. Akiyama, Improvement in thermal endurance of D-mannitol as phase-change material by impregnation into nanosized pores, Mater. Chem. Phys. 146 (3) (2014) 253–260, https://doi.org/10.1016/j.matchemphys.2014.03.009, ago.

[9] S. Salyan, S. Suresh, A.S. Reddy, Low melt alloy enhanced solid-liquid phase change organic sugar alcohol for solar thermal energy storage, J. Mol. Liq. 266 (sep. 2018) 29–42, https://doi.org/10.1016/j.molliq.2018.06.002.

[10] N. Beemkumar, A. Karthikeyan, B. Saravanakumar, J. Jayaprabakar, Performance improvement of D-sorbitol PCM-based energy storage system with different fins, Int. J. Ambient Energy 39 (4) (may 2018) 372–376, https://doi.org/10.1080/01430750.2017.1303642.

[11] J. Saroha, S. Mehra, M. Kumar, S. Sharma, Thermo-physical properties of paraffin/TiO2 and sorbitol/TiO2 nanocomposites for enhanced phase change materials: a study on the stability issue, Appl. Phys. A 127 (12) (2021) 916, https://doi.org/10.1007/s00339-021-05050-2, dic.

[12] J. Kasitz, A. Vargas, H. Carlton, D. Huitink, Nanoparticle enhanced crystallization of sorbitol PCMs for latent heat and temperature control, in: en *2020 19th IEEE Intersociety Conference on Thermal and Thermomechanical Phenomena in Electronic Systems*, ITherm, Orlando, FL, USA, jul. 2020, pp. 690–696, https://doi.org/10.1109/ITherm45881.2020.9190536.

[13] V. Sobhansarbandi, Performance optimization of thermal energy storage based solar collector, ASME 2021 Power Conf (jul. 2021), https://doi.org/10.1115/power2021-64127.

[14] A. Kaizawa, et al., Thermophysical and heat transfer properties of phase change material candidate for waste heat transportation system, Heat Mass Tran. 44 (7) (may 2008) 763–769, https://doi.org/10.1007/s00231-007-0311-2.

[15] G. Diarce, I. Gandarias, A. Campos, A. Garcia, U. Griesser, Eutectic mixtures of sugar alcohols for thermal energy storage in the 50–90°C temperature range, Sol. Energy Mater. Sol. Cells 134 (mar. 2015) 215–226, https://doi.org/10.1016/j.solmat.2014.11.050.

[16] H. Zhang, et al., Experimental and in silico characterization of xylitol as seasonal heat storage material, Fluid Phase Equil. 436 (mar. 2017) 55–68, https://doi.org/10.1016/j.fluid.2016.12.020.

[17] A. Seppala, K. Turunen, M. Yazdani, Thermal conductivity of sugar alcohols, Sol. Energy Mater. Sol. Cells 243 (2022), https://doi.org/10.1016/j.solmat.2022.111796, 111796-111796, ago.

[18] S. Tomassetti, et al., A review on thermophysical properties and thermal stability of sugar alcohols as phase change materials, J. Energy Storage 55 (nov. 2022), 105456, https://doi.org/10.1016/j.est.2022.105456.

[19] S. Hohlein, A. Konig, D. Bruggemann, Thermophysical characterization of $MgCl_2{\cdot}6H_2O$, xylitol and erythritol as phase change materials (PCM) for latent heat thermal energy storage (LHTES), Materials 10 (4) (2017) 444, https://doi.org/10.3390/ma10040444.

[20] P. del Barrio, et al., Characterization of different sugar alcohols as phase change materials for thermal energy storage applications, Sol. Energy Mater. Sol. Cells 159 (2017) 560–569, https://doi.org/10.1016/j.solmat.2016.10.009.

[21] R. Jia, et al., Heat capacities of some sugar alcohols as phase change materials for thermal energy storage applications, J. Chem. Thermodyn. 115 (2017) 233–248, https://doi.org/10.1016/j.jct.2017.08.004, dic.

[22] M. Dannemand, J.M. Schultz, J.B. Johansen, S. Furbo, Long term thermal energy storage with stable supercooled sodium acetate trihydrate, Appl. Therm. Eng. 91 (2015) 671–678, https://doi.org/10.1016/j.applthermaleng.2015.08.055, dic.

[23] G. Englmair, C. Moser, S. Furbo, M. Dannemand, J. Fan, Design and functionality of a segmented heat-storage prototype utilizing stable supercooling of sodium acetate trihydrate in a solar heating system, Appl. Energy 221 (jul. 2018) 522–534, https://doi.org/10.1016/j.apenergy.2018.03.124.

[24] R. Anish, V. Mariappan, S. Suresh, M.M. Joybari, A.M. Abdulateef, Experimental investigation on the energy storage/discharge performance of xylitol in a compact spiral coil heat exchanger, Int. J. Therm. Sci. 159 (2021), 106633, https://doi.org/10.1016/j.ijthermalsci.2020.106633 ene.

[25] M.R. Yazdani, J. Etula, J.B. Zimmerman, A. Seppala, Ionic cross-linked polyvinyl alcohol tunes vitrification and cold-crystallization of sugar alcohol for long-term thermal energy storage, Green Chem. 22 (16) (2020) 5447–5462, https://doi.org/10.1039/d0gc01427c, ago.

[26] G. Coccia, A. Aquilanti, A. Aquilanti, S. Tomassetti, Pio Francesco, G. Di Nicola, Experimental analysis of nucleation triggering in a thermal energy storage based on xylitol used in a portable solar box cooker, Energies 14 (18) (sep. 2021) 5981, https://doi.org/10.3390/en14185981.

[27] J. An, et al., Novel sugar alcohol/carbonized kapok fiber composites as form-stable phase-change materials with exceptionally high latent heat for thermal energy storage, ACS Omega 4 (3) (mar. 2019) 4848–4855, https://doi.org/10.1021/acsomega.8b03373.

[28] S. Agrawal, A. Paterson, Secondary nucleation: mechanisms and models, Chem. Eng. Commun. 202 (5) (2015) 698–706, https://doi.org/10.1080/00986445.2014.969369, ene.

[29] L. Bosetti, M. Mazzotti, M. Mazzotti, Population balance modeling of growth and secondary nucleation by attrition and ripening, Cryst. Growth Des. 20 (1) (2020) 307–319, https://doi.org/10.1021/acs.cgd.9b01240, ene.

[30] S.G. Agrawal, A. Balandier, A. Paterson, J.R. Jones, Study on lactose attrition inside the mixing cell of a laser diffraction particle sizer using a novel attrition index, Powder Technol. 208 (3) (2011) 669–675, https://doi.org/10.1016/j.powtec.2011.01.007, abr.

[31] J. Wang, J. Estrin, Secondary nucleation of sucrose by fluid shear in aqueous solutions, Chem. Eng. Commun. 152–153 (1) (oct. 1996) 275–286, https://doi.org/10.1080/00986449608936568.

[32] T. Speck, The role of shear in crystallization kinetics: from suppression to enhancement, Sci. Rep. 5 (1) (nov. 2015), 14610, https://doi.org/10.1038/srep14610.

[33] A. Seppala, A. Merilainen, L. Wikstrom, P. Kauranen, The effect of additives on the speed of the crystallization front of xylitol with various degrees of supercooling, Exp. Therm. Fluid Sci. 34 (5) (jul. 2010) 523–527, https://doi.org/10.1016/j.expthermflusci.2009.11.005.

[34] N. Beaupere, N. Beaupere, U. Soupremanien, L. Zalewski, L. Zalewski, Nucleation triggering methods in supercooled phase change materials (PCM), a review, Thermochim. Acta 670 (2018) 184–201, https://doi.org/10.1016/j.tca.2018.10.009, dic.

[35] A. Godin, M. Duquesne, E.P. del Barrio, F. Achchaq, P. Monneyron, Bubble agitation as a new low-intrusive method to crystallize glass-forming materials,

Energy Proc. 139 (2017) 352–357, https://doi.org/10.1016/j.egypro.2017.11.220, dic.

[36] M. Duquesne, E.P. del Barrio, E.P. Del Barrio, A. Godin, Nucleation triggering of highly undercooled xylitol using an air lift reactor for seasonal thermal energy storage, Appl. Sci. 9 (2) (2019) 267, https://doi.org/10.3390/app9020267.

[37] Louis Piquard, Emilie Gagniere, Gregory Largiller, Denis Mangin, F. Bentivoglio, Xylitol used as phase change material: nucleation mechanisms of the supercooling rupture by stirring, J. Energy Storage 48 (2022), https://doi.org/10.1016/j.est.2021.103922, 103922-103922, abr.

[38] A.M. Omran, C.J. King, Kinetics of ice crystallization in sugar solutions and fruit juices, AIChE J. 20 (4) (jul. 1974) 795–803, https://doi.org/10.1002/aic.690200422.

[39] A.S. Myerson, D. Erdemir, A.Y. Lee (Eds.), Handbook of Industrial Crystallization, 3.ª ed., Cambridge University Press, 2019 https://doi.org/10.1017/9781139026949.